Delft University of Technology

Multi-epoch PPP-RTK corrections

temporal characteristics, pitfalls and user-impact

Psychas, D.; Khodabandeh, A.; Teunissen, P. J.G.

Important note
To cite this publication, please use the final published version (if applicable).
Please check the document version above.

ORIGINAL ARTICLE

Multi-epoch PPP-RTK corrections: temporal characteristics, pitfalls and user-impact

D. Psychas[1] · A. Khodabandeh[2] · P. J. G. Teunissen[2,3,4]

Abstract

PPP-RTK corrections, aiding GNSS users to achieve single-receiver integer ambiguity-resolved parameter solutions, are often estimated in a recursive manner by a provider. Such recursive, multi-epoch, estimation of the corrections relies on a set of $\mathcal{S}$-basis parameters that are chosen by the provider so as to make the underlying measurement setup solvable. As a consequence, the provider can only estimate *estimable* forms of the corrections rather than the original corrections themselves. It is the goal of the present contribution to address the consequence of the corrections' dependency on the provider's $\mathcal{S}$-basis, showcasing the characteristics of their multi-epoch solutions, thereby identifying potential pitfalls which the PPP-RTK user should avoid when evaluating such solutions. To this end, we develop a simulation platform that allows one to have full control over the properties of PPP-RTK corrections and demonstrate various misleading temporal behaviors that exist when interpreting the multi-epoch solutions of their estimable forms. The roles of the correction latency and time correlation in the multi-epoch user positioning performance are quantified, while the deviation of the user-reported positioning precision description from its user-actual counterpart is measured under a misspecified user stochastic model.

Keywords Global navigation satellite systems (GNSS) · PPP-RTK corrections · Multi-epoch filtering · Correction latency · Time correlation · Integer ambiguity resolution (IAR)

1 Introduction

The transition from the precise point positioning (PPP) concept (Heroux and Kouba 1995; Zumberge et al. 1997) to its integer ambiguity resolution-enabled variant (PPP-RTK; Wübbena et al. 2005) is realized by providing single-receiver users, next to the network-derived satellite orbits and clocks, with information about the satellite biases. Their role is to construct integer-estimable user ambiguities and enable single-receiver carrier-phase ambiguity resolution. The set of the PPP-RTK corrections may also optionally contain atmo-spheric delays so as to speed up the user convergence (Li et al. 2011; Psychas and Verhagen 2020; Zha et al. 2021). Such corrections can be determined and delivered to the users from a provider that may utilize either a multi- or a single-station setup (Khodabandeh and Teunissen 2015). Several PPP-RTK methods have been formulated and proposed in the past, see, e.g., Ge et al. (2008), Collins (2008), Mervart et al. (2008), Laurichesse et al. (2009), Teunissen et al. (2010), Geng et al. (2012) and Odijk et al. (2016).

Although each model provides a different set of corrections, the estimability analysis of Teunissen and Khodabandeh (2015) showed, first, that a careful interpretation of the estimable corrections is crucial in properly understanding the PPP-RTK mechanization and, second, that their information content is the same. Despite the different parametrizations used, the corresponding *estimable* parameters act as if they are the *original* parameters with which the users need to correct their observables. However, this does not necessarily imply that such estimable parameters will have the *same* first moment and behavior as those of their original counterparts. This is because of the various offsets by which the original parameters are biased and the dynamic model settings

✉ D. Psychas
dimitrios.psychas@ext.esa.int

1 European Space Agency (ESA/ESTEC), Noordwijk, The Netherlands

2 Department of Infrastructure Engineering, University of Melbourne, Melbourne, Australia

3 Department of Geoscience and Remote Sensing, Delft University of Technology, Delft, The Netherlands

4 GNSS Research Centre, Curtin University of Technology, Perth, Australia

used by the providers' filter. While one can infer the statistical characteristics of such estimable parameter solutions from their closed-form variance matrices (Khodabandeh and Teunissen 2015), we will show that a cursory numerical illustration of their characteristics over time can become misleading. Misleading impressions would be caused by interpreting only a single sample of the PPP-RTK solutions out of infinitely many 'realizations' whose time correlation is considerably large. To effectively pinpoint potential pitfalls when interpreting the solutions, one may therefore take recourse to a simulation platform, generating a large number of such realizations. This is the approach that will be pursued by the present contribution.

Correction providers often establish multi-epoch filter setups to compute individual PPP-RTK solutions and disseminate a subset of the solutions (i.e., the corrections) to users, see, e.g., Henkel et al. (2010), Zhang et al. (2011) and Wang et al. (2017). Multi-epoch filtering is employed for two main reasons: first, to enable the corrections to become more precise over time and, second, to augment velocity (or drift) parameters by which users are able to bridge the gap between the correction generation time and the user positioning time, thereby also reducing the corrections' transmission rate. An analysis of the quality of the PPP-RTK corrections and how this is driven by the information content and adjustment of a network setup has been presented in Khodabandeh and Teunissen (2015), highlighting also the high correlation between the individual corrections. The impact of discarding the stochasticity of the PPP-RTK corrections has been shown to be considerable in both the ambiguity resolution (Khodabandeh 2021) and the positioning domain (Psychas et al. 2022) under large latencies in a single-epoch user setup.

When it comes to a user multi-epoch formulation, one needs to recall that the usage of a dynamic model in the provider-filter will deliver parameter solutions that are inherently correlated in time. This property is often neglected in the user-filter as it is tacitly assumed that the temporal correlation of the corrections decays rapidly over time and does not significantly impact the user parameter solutions and, therefore, can be safely ignored. Despite often neglecting this stochastic contribution, there are studies demonstrating that ambiguity resolution can still be successfully realized, see, e.g., Duong et al. (2019), Psychas and Verhagen (2020), Geng et al. (2022), Hou and Zhang (2023). Khodabandeh et al. (2023) has developed a user-filter able to deliver close-to-minimum-variance solutions, by treating the corrections as additional observations, given that the duration of the provider-filter initialization is sufficiently large. Would the PPP-RTK user want to obtain minimum-variance parameter solutions in a multi-epoch setup, the correctly-specified stochastic model of the corrected data, including time correlation, needs to be incorporated into the estimation process.

The present contribution aims to provide a systematic analysis of the *multi-epoch filtered* PPP-RTK corrections and their characteristics by presenting a precision and temporal correlation analysis as a function of their latency and the provider's dynamic model settings. Next to the insight provided by the analysis, we demonstrate the pitfalls that exist when analyzing only a single sample of the estimable parameter solutions at the undifferenced level. This is realized through a simulation environment we developed that allows one to have full control over the observation model and the (known and estimated) GNSS parameters, thereby giving one the capability to evaluate the consequences of the assumptions made on the temporal behavior of the parameters. Particular emphasis is then given to the aspect of time correlation that the multi-epoch-filtered corrections are subject to. To this end, we numerically demonstrate whether or not this property can be safely ignored and to what extent the user-reported quality information under a misspecified correctional stochastic regime differs from its user-actual counterpart.

2 Simulation platform

In this section, we present the underlying measurement and dynamic models on which our simulation platform is based. The functionality of the platform is twofold. First, multiple time-series of the parameters and the measurements are generated and registered as true values. Second, a Kalman filter is formulated to recursively compute *estimable forms* of the parameters, thereby evaluating the parameter estimation errors through the comparison of the estimated values with their true versions. The way both the sets of parameters and measurements are simulated is discussed, followed by the structure of the Kalman filter setup employed.

2.1 Parameters generated as random processes

Although one is allowed to make any plausible assumption on the temporal behavior of the involved parameters in a simulation framework, we attempt in our simulation to align with temporal characteristics that have already been reported in the literature. Accordingly, the carrier-phase integer ambiguities from satellite s ($s = 1, \ldots, m$) to the provider receiver r, on frequency j ($j = 1, \ldots, f$), are denoted by $a_{r,j}^s$ and assumed to be constant in time, unless cycle slips occur. On the other hand, the frequency-dependent phase receiver and satellite biases, at epoch k, are denoted by $\delta_{r,j}(k)$ and $\delta_{,j}^s(k)$, and assumed to behave stable over time. A random-walk constant-state process with a zero-mean system noise is utilized to model their temporal behavior. Likewise, the temporal behavior of the corresponding code biases $d_{r,j}(k)$ and $d_{,j}^s(k)$ is captured by constant-state processes (Komjathy

et al. 2005; Zhang et al. 2018). The stated parameters can therefore be simulated over time as follows:

$$
\begin{cases}
a_{r,j}^s(k) = a_{r,j}^s \text{ (arbitrary integer)} \\
\delta_{r,j}(k) = \delta_{r,j}(k-1) + n_{\delta_{r,j}}(k) \\
\delta_{\cdot,j}^s(k) = \delta_{\cdot,j}^s(k-1) + n_{\delta_{\cdot,j}^s}(k) \\
d_{r,j}(k) = d_{r,j}(k-1) + n_{d_{r,j}}(k) \\
d_{\cdot,j}^s(k) = d_{\cdot,j}^s(k-1) + n_{d_{\cdot,j}^s}(k)
\end{cases}
\tag{1}
$$

for $k = 2, \ldots, K$, with K being the total number of epochs. The system noise of parameter $(\cdot)$ is denoted by $n_{(\cdot)}$ which can be sampled from zero-mean Gaussian noises (Teunissen 2007). Arbitrary initial values are assigned to each parameter at epoch $k = 1$. The system noise standard deviations of the code and phase biases are set to zero.

As for the satellite clocks $dt^s(k)$ and first-order slant ionospheric delays $\iota_r^s(k)$, a constant-velocity process with extra velocity parameters (∂dt^s and $\partial \iota_r^s$) is utilized to model their time-variation (Wang et al. 2017). However, it is assumed that constant-velocity processes may not properly capture the highly dynamic time-variability of the receiver clock $dt_r(k)$, leaving $dt_r(k)$ with no dynamic model. The time series of these parameters is therefore generated as follows:

$$
\begin{cases}
dt_r(k) = \text{ arbitrary value at every epoch} \\
dt^s(k) = dt^s(k-1) + \Delta t \, \partial dt^s(k-1) + n_{dt^s}(k) \\
\partial dt^s(k) = \partial dt^s(k-1) + n_{\partial dt^s}(k) \\
\iota_r^s(k) = \iota_r^s(k-1) + \Delta t \, \partial \iota_r^s(k-1) + n_{\iota_r^s}(k) \\
\partial \iota_r^s(k) = \partial \iota_r^s(k-1) + n_{\partial \iota_r^s}(k)
\end{cases}
\tag{2}
$$

for $k = 2, \ldots, K$, with Δt being the sampling interval. As with (1), arbitrary initial values are assigned to each parameter at epoch $k = 1$, while the corresponding system noises follow the zero-mean Gaussian distribution. The system noise standard deviations of the clock and ionospheric acceleration parameters are set to 3 mm/$\sqrt{\text{s}^3}$ and 0.5 mm/$\sqrt{\text{s}^3}$, respectively. It is important to remark that the system noises are required to be *uncorrelated* over time in accordance with the Kalman filter's standard assumptions. Here and in the following, the receiver and satellite position vectors, x_r and x^s, are assumed to be known.

2.2 Forming the measurements

Once the true values of the parameters are simulated, one can follow the GNSS observation equations (Teunissen and Montenbruck 2017) and structure the corresponding measurements. Let $\phi_{r,j}^s(k)$ and $p_{r,j}^s(k)$ denote the carrier-phase and pseudo-range (code) measurements, respectively. By computing the geometric satellite-to-receiver distance $||x_r - x^s||$, lumped with the slant tropospheric delay τ_r^s, i.e., $\rho_r^s = ||x_r - x^s|| + \tau_r^s$, the stated measurements are simulated

as follows:

$$
\begin{cases}
\phi_{r,j}^s(k) = \rho_r^s(k) + dt_r(k) - dt^s(k) - \mu_j \iota_r^s(k) \\
\quad + \lambda_j(\delta_{r,j}(k) - \delta_{\cdot,j}^s(k) + a_{r,j}^s) + \epsilon_{\phi_{r,j}^s}(k); \\
p_{r,j}^s(k) = \rho_r^s(k) + dt_r(k) - dt^s(k) + \mu_j \iota_r^s(k) \\
\quad + d_{r,j}(k) - d_{\cdot,j}^s(k) + \epsilon_{p_{r,j}^s}(k)
\end{cases}
\tag{3}
$$

for $k = 1, \ldots, K$. The first-order slant ionospheric delay ι_r^s is linked to the measurements via the frequency-dependent ratios $\mu_j = \lambda_j^2/\lambda_1^2$ that are driven by the wavelengths λ_j ($j = 1, \ldots, f$). Note, apart from $\delta_{r,j}$, $\delta_{\cdot,j}^s$ and $a_{r,j}^s$ that are expressed in cycles, that the rest of the quantities are all in units of length. To accommodate the Kalman filter's standard assumptions, the Gaussian zero-mean measurement noises $\epsilon_{\phi_{r,j}^s}(k)$ and $\epsilon_{p_{r,j}^s}(k)$ are assumed to be 'uncorrelated' in time and uncorrelated with the parameters' system noises. Their standard deviations (STDs) are assumed to be dependent on satellite elevation and are considered equal at all frequencies. An exponential elevation weighting strategy with the zenith-referenced STDs of 2 mm (phase) and 20 cm (code) is employed to model the STDs of the measurement noises.

2.3 Kalman filter's measurement and dynamic models

Now that the simulated measurements (3) are formed, the task is to estimate the parameters with the aid of the multi-epoch dynamic models (1) and (2). Ideally, one aims at estimating all the parameters involved. Due to the existing rank deficiencies in the system of undifferenced GNSS observation equations (3), one can, however, only estimate a subset of the parameters. The remaining parameters have to be held fixed as $\mathcal{S}$-basis so as to form the minimum constraints of the model (Odijk et al. 2016). As a consequence, the $\mathcal{S}$-basis parameters will be absorbed by the estimable parameters, forming a full-rank system of measurement and dynamic models that can be applicable to a Kalman filter setup.

Let $\Delta\phi_{r,j}^s(k) = \phi_{r,j}^s(k) - \rho_r^s$ and $\Delta p_{r,j}^s(k) = p_{r,j}^s(k) - \rho_r^s$ be the 'observed-minus-computed' measurements. The provider filter's measurement model, in its full-rank form, reads (Khodabandeh 2021)

Measurement model ($k = 1, \ldots, K$)
$$
\begin{cases}
\Delta\phi_{r,j}^s(k) = d\tilde{t}_r(k) - d\tilde{t}^s(k) - \mu_j \tilde{\iota}_r^s(k) \\
\quad + \lambda_j(\tilde{\delta}_{r,j}(k) - \tilde{\delta}_{\cdot,j}^s(k)) + \epsilon_{\phi_{r,j}^s}(k); \\
\Delta p_{r,j}^s(k) = d\tilde{t}_r(k) - d\tilde{t}^s(k) + \mu_j \tilde{\iota}_r^s(k) \\
\quad + \tilde{d}_{r,j}(k) - \tilde{d}_{\cdot,j}^s(k) + \epsilon_{p_{r,j}^s}(k)
\end{cases}
\tag{4}
$$

that is accompanied by the provider filter's dynamic models

Table 1 Estimable parameters and $\mathcal{S}$-basis parameters of the single-system, multi-frequency, single-station provider model, in case of the constant-velocity setup for the satellite clocks and ionospheric delays

Parameter	Interpretation
Rec. clocks	$d\tilde{t}_r(k) = dt_r(k) - dt_r(1) - [k-1]\Delta t \, \partial d\bar{t}_r$
Sat. clocks	$d\tilde{t}^s(k) = dt^s(k) + d^s_{,\mathrm{IF}}(1) - dt_r(1) - d_{r,\mathrm{IF}}(1) - [k-1]\Delta t \, \partial d\bar{t}_r - \tau^s_r(k)$
Ionospheric delays	$\tilde{\iota}^s_r(k) = \iota^s_r(k) + d_{r,\mathrm{GF}}(1) - d^s_{,\mathrm{GF}}(1)$
Rec. phase biases	$\tilde{\delta}_{r,j}(k) = \delta_{r,j}(k) - \delta_{r,j}(1)$
Sat. phase biases	$\tilde{\delta}^s_{,j}(k) = \delta^s_{,j}(k) + \frac{1}{\lambda_j}\left(\mu_j[d^s_{,\mathrm{GF}}(1) - d_{r,\mathrm{GF}}(1)] - [d^s_{,\mathrm{IF}}(1) - d_{r,\mathrm{IF}}(1)]\right) - \delta_{r,j}(1) - a^s_{r,j}$
Rec. code biases	$\tilde{d}_{r,j}(k) = d_{r,j}(k) - d_{r,j}(1)$
Sat. code biases	$\tilde{d}^s_{,j}(k) = \begin{cases} d^s_{,j}(k) - d^s_{,j}(1); \ j = 1,2 \\ [d^s_{,j}(k) - (d^s_{,\mathrm{IF}}(1) + \mu_j d^s_{,\mathrm{GF}}(1))] - [d_{r,j}(1) - (d_{r,\mathrm{IF}}(1) + \mu_j d_{r,\mathrm{GF}}(1))]; \ j > 2 \end{cases}$
Ionospheric velocities	$\partial \tilde{\iota}^s_r(k) = \partial \iota^s_r(k)$
Sat. clock velocities	$\partial d\tilde{t}^s(k) = \partial dt^s(k) - \partial d\bar{t}_r$
Rec. clock velocities*	$\partial d\tilde{t}_r(k) = \partial dt_r(k) - \partial d\bar{t}_r$ (*if a constant-velocity setup is assumed for dt_r as well)
$\mathcal{S}$-basis parameters	$dt_r(1), \ dt_r(2), \ d_{r,j}(1), \ \delta_{r,j}(1), \ d^s_{,j=1,2}(1), \ a^s_{r,j}$

$(\cdot)_{,\mathrm{IF}} = \frac{1}{\mu_2-\mu_1}[\mu_2(\cdot)_{,1} - \mu_1(\cdot)_{,2}]; \quad (\cdot)_{,\mathrm{GF}} = \frac{1}{\mu_2-\mu_1}[(\cdot)_{,2} - (\cdot)_{,1}], \quad \partial d\bar{t}_r = \frac{1}{\Delta_t}[dt_r(2) - dt_r(1)]$

Dynamic model ($k = 2, \ldots, K$)

$$\begin{cases} \tilde{\delta}_{r,j}(k) = \tilde{\delta}_{r,j}(k-1) + n_{\delta_{r,j}}(k) \\ \tilde{\delta}^s_{,j}(k) = \tilde{\delta}^s_{,j}(k-1) + n_{\delta^s_{,j}}(k) \\ \tilde{d}_{r,j}(k) = \tilde{d}_{r,j}(k-1) + n_{d_{r,j}}(k) \\ \tilde{d}^s_{,j}(k) = \tilde{d}^s_{,j}(k-1) + n_{d^s_{,j}}(k) \end{cases} \quad (5)$$

and

$$\begin{cases} d\tilde{t}^s(k) = d\tilde{t}^s(k-1) + \Delta t \, \partial d\tilde{t}^s(k-1) + n_{dt^s}(k) \\ \partial d\tilde{t}^s(k) = \partial d\tilde{t}^s(k-1) + n_{\partial dt^s}(k) \\ \tilde{\iota}^s_r(k) = \tilde{\iota}^s_r(k-1) + \Delta t \, \partial \tilde{\iota}^s_r(k-1) + n_{\iota^s_r}(k) \\ \partial \tilde{\iota}^s_r(k) = \partial \tilde{\iota}^s_r(k-1) + n_{\partial \iota^s_r}(k) \end{cases} \quad (6)$$

In the system of equations (4), (5) and (6), the role of the original parameters is taken by their estimable forms distinguished by the tilde symbol $\tilde{\cdot}$. They are formed by a choice of $\mathcal{S}$-basis. Table 1 presents such $\mathcal{S}$-basis parameters and shows how these estimable parameters are linked to their original counterparts. For instance, the table indicates that the ionosphere velocity parameters can be *unbiasedly* determined by the provider filter, that is $\partial \tilde{\iota}^s_r(k) = \partial \iota^s_r(k)$. This is, however, not the case with the satellite clock velocity parameters. Since the receiver clock parameters of the first two epochs $dt_r(k)$ ($k = 1, 2$) are taken as $\mathcal{S}$-basis, they are absorbed by the estimable clock velocity parameters as $\partial d\tilde{t}^s(k) = \partial dt^s(k) - \partial d\bar{t}_r$, where $\partial d\bar{t}_r = [dt_r(2) - dt_r(1)]/\Delta t$. In the next section, it is illustrated why such subtle differences between the interpretations of the PPP-RTK estimable parameters need to be properly accounted for.

3 Corrections and their solutions

Considering the simulated parameters in (1) and (2) as true values, the estimation performance of the provider filter in delivering PPP-RTK corrections can now be investigated. Such investigation is infeasible in real-world experiments due to the fact that the original and estimable parameters are unknown. We present the single-station PPP-RTK parameter solutions and analyze their temporal behavior, consistency with their original counterparts and their time correlation feature. Although here we made use of a single-station correction provider setup, this does not affect the generality of our analysis, as the aforementioned concept can be naturally carried over to the multi-station setup.

3.1 Provider parameter solutions

Although only the estimators of the PPP-RTK corrections are relevant for aiding the user in realizing single-receiver ambiguity resolution, a comprehensive analysis of the estimable receiver clock, as part of the PPP-RTK parameter solutions, takes place in this section to identify and characterize any potential pitfalls one may be led to in, e.g., timing applications. The principal advantage of the current simulation analysis over a real-data experiment is that we have complete control over the properties to be studied. Next to that, such an analysis can shed light into the errors of the estimated parameters since the true parameters are a priori known in the simulation platform.
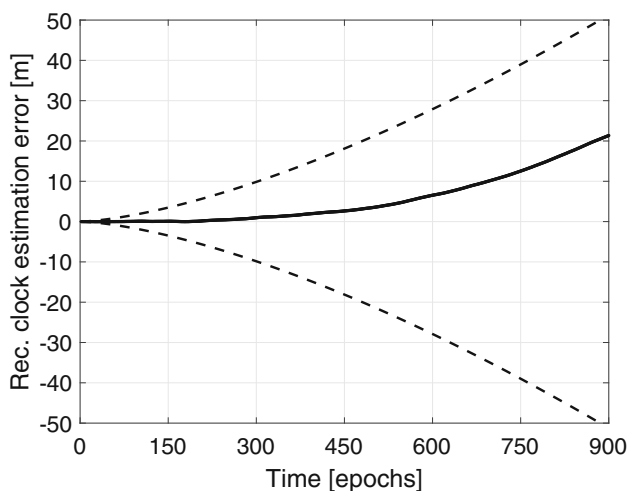
Fig. 1 Time-series of the receiver clock estimation error (solid line) and its 99.9% confidence interval (dashed lines) for the single-station provider, under a constant-velocity setup for the satellite clocks
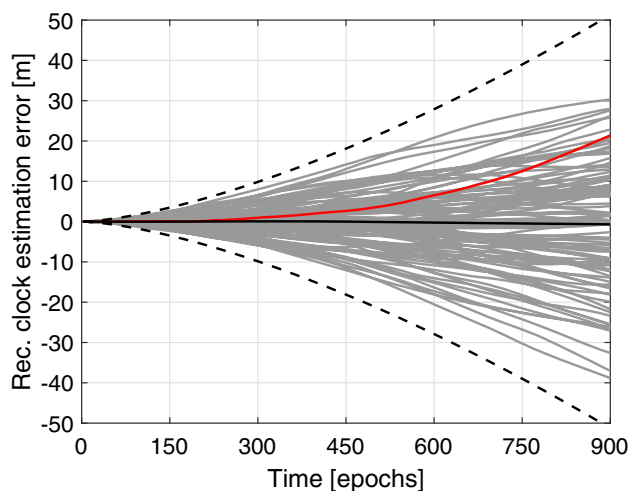

Fig. 2 Time-series of the receiver clock estimation error (gray solid lines) and its 99.9% confidence interval for independent Kalman filter realizations of 100 normally-distributed observation samples, under a constant-velocity setup for the satellite clocks. Their mean value is indicated by the black solid line. The line highlighted in red depicts the single realization of the receiver clock solutions shown in Fig. 1

3.1.1 Receiver clock

We commence our analysis with the receiver clock parameter solutions. Our initial assumption on an unlinked-in-time receiver clock led to the estimable parameters shown in Table 1, in which the receiver clock that the Kalman filter delivers is biased by the clock value at the first epoch and an ever-increasing second term that involves the receiver clock velocity term $\partial d\bar{t}_r$. Since the estimable receiver clock $d\tilde{t}_r(k)$ at any epoch k has been determined from the combination of the parameters $dt_r(k)$, $dt_r(1)$, and $dt_r(2)$, one may be inclined to expect its Kalman-filter estimate $d\hat{\tilde{t}}_r(k)$ to converge to its true value $d\tilde{t}_r(k)$. However, Fig. 1 refutes such expectation. The figure shows that the time-series of the estimation error $d\hat{\tilde{t}}_r(k) - d\tilde{t}_r(k)$ systematically diverges from the expected zero value over time. This behavior is also echoed by the confidence intervals of the estimable receiver clock. With reference to the *unbiasedness* property of the solutions output by the provider filter, a cursory glance at the time-series in Fig. 1 may incline one to conclude that the provider filter is misspecified, delivering *biased* solutions. However, one should be noted that the *unbiasedness* property $\mathsf{E}(d\hat{\tilde{t}}_r(k)) = \mathsf{E}(d\tilde{t}_r(k))$, with $\mathsf{E}(\cdot)$ being the expectation operator, states that the clock estimation error $d\hat{\tilde{t}}_r(k) - d\tilde{t}_r(k)$ must be zero mean at a given single epoch k.

This apparent paradox can be addressed by the fact that multi-epoch parameter solutions are *random processes*, while the filter only delivers a sample out of their infinitely many *realizations*. Therefore, the property $\mathsf{E}(d\hat{\tilde{t}}_r(k) - d\tilde{t}_r(k)) = 0$ can be visualized only after accumulating multiple Kalman filter realizations, as shown in Fig. 2. We simulated 100 independent sets of GNSS observables under the same setup. As

shown, their mean value is close to zero (black solid line). That the realizations of the receiver clock solution diverge from their expected value indicates that the *variance* of the receiver clock solution incrementally increases over time under the measurement and dynamic models (4) and (5).

In understanding the behavior of the formal error variance of the receiver clock, let us make a few simplifications for the sake of presentation. According to Table 1, the estimable receiver biases $\tilde{\delta}_{r,j}(k)$ and $\tilde{d}_{r,j}(k)$ are in fact the *time differences* of their original counterparts. They are therefore constrained to be zero when setting their system noises to zero. For this special case, such biases are thus absent. This is also the case with satellite code biases on the first two frequencies $j = 1, 2$. Moreover, as the geometry-free (GF) combined measurements serve for the determination of the estimable ionospheric delays, we only focus on the (ionosphere-free) IF combined measurements. Likewise, the epoch argument k is omitted for the satellite biases as they are assumed to be time-constant. Accordingly, the IF version of the full-rank version of (4) reads

$$\begin{aligned} \mathsf{E}(\Delta\phi^s_{r,\mathrm{IF}}(k)) &= d\tilde{t}_r(k) - d\tilde{t}^s(k) - \tilde{\delta}^s_{,\mathrm{IF}} \\ \mathsf{E}(\Delta p^s_{r,\mathrm{IF}}(k)) &= d\tilde{t}_r(k) - d\tilde{t}^s(k) \end{aligned} \tag{7}$$

According to the canonical differencing transformation (Khodabandeh and Teunissen 2017), the estimable satellite clocks $d\tilde{t}^s$ are formed as the summation of their *satellite-averaged* component $d\tilde{t}^{\bar{s}} = (1/m)\sum_{i=1}^{m} d\tilde{t}^i$ and their *single-differenced* (SD) component $d\tilde{t}^{s\bar{s}} = d\tilde{t}^s - d\tilde{t}^{\bar{s}}$, that is, $d\tilde{t}^s = d\tilde{t}^{s\bar{s}} + d\tilde{t}^{\bar{s}}$. We now show that it is the solution's variance of the satellite-averaged component $d\tilde{t}^{\bar{s}}$ that increases

in time, leading to variance increase in both the estimable receiver and satellite clocks $d\tilde{t}_r$ and $d\tilde{t}^s$, respectively. In the *absence* of the phase observations, the system of equations corresponding to the filter's initialization ($k = 1, 2$) reads

$$
\begin{aligned}
\mathsf{E}(\Delta p_{r,\mathrm{IF}}^{\bar{s}}(1)) &= -d\tilde{t}^{\bar{s}}(1) \\
\mathsf{E}(\Delta p_{r,\mathrm{IF}}^{\bar{s}}(2)) &= -d\tilde{t}^{\bar{s}}(2) \\
\mathsf{E}(n_{dt^{\bar{s}}}(2)) &= +d\tilde{t}^{\bar{s}}(2) - d\tilde{t}^{\bar{s}}(1) - \Delta t \, \partial d\tilde{t}^{\bar{s}}(1) \\
\mathsf{E}(n_{\partial dt^{\bar{s}}}(2)) &= +\partial d\tilde{t}^{\bar{s}}(2) - \partial d\tilde{t}^{\bar{s}}(1)
\end{aligned}
\tag{8}
$$

As the number of unknowns are equal to the number of equations, the solution follows from direct substitution, that is, $d\hat{\tilde{t}}^{\bar{s}}(k) = -\Delta p_{r,\mathrm{IF}}^{\bar{s}}(k)$ ($k = 1, 2$), $\partial d\hat{\tilde{t}}^{\bar{s}}(1) = (1/\Delta t)(d\hat{\tilde{t}}^{\bar{s}}(2) - d\hat{\tilde{t}}^{\bar{s}}(1) - n_{dt^{\bar{s}}}(2))$, and $\partial d\hat{\tilde{t}}^{\bar{s}}(2) = \partial d\hat{\tilde{t}}^{\bar{s}}(1) + n_{\partial dt^{\bar{s}}}(2)$. From the third epoch onward ($k \geq 3$), the new unknowns $d\tilde{t}_r(k)$ come into play. As a consequence, the observations $\Delta p_{r,\mathrm{IF}}^{\bar{s}}(k)$, and the pseudo-observations $n_{dt^{\bar{s}}}(k)$ and $n_{\partial dt^{\bar{s}}}(k)$ are *fully* reserved for $d\tilde{t}_r(k)$, $d\tilde{t}^{\bar{s}}(k)$ and $\partial d\tilde{t}^{\bar{s}}(k)$, respectively. This means, in the absence of phase observations, that there is *no* redundancy in the system of satellite-averaged IF code observations. Therefore, the solution for the satellite-averaged component follows as

$$
\begin{aligned}
d\hat{\tilde{t}}^{\bar{s}}(k) &= d\hat{\tilde{t}}^{\bar{s}}(k-1) + \Delta t \, \partial d\hat{\tilde{t}}^{\bar{s}}(k-1) + n_{dt^{\bar{s}}}(k) \\
&= d\hat{\tilde{t}}^{\bar{s}}(2) + \Delta t \left(\sum_{i=2}^{k-1} \partial d\hat{\tilde{t}}^{\bar{s}}(i)\right) + \sum_{i=3}^{k} n_{dt^{\bar{s}}}(i),
\end{aligned}
\tag{9}
$$

while the receiver clock solutions read $d\hat{\tilde{t}}_r(k) = \Delta p_{r,\mathrm{IF}}^{\bar{s}}(k) + d\hat{\tilde{t}}^{\bar{s}}(k)$. According to the second expression of (9), the process noises $n_{dt^{\bar{s}}}(i)$ ($i = 3, \ldots, k$) are cumulatively added to the solution of $d\hat{\tilde{t}}^{\bar{s}}(k)$, increasing its variance in time. Now assume that the phase observations $\Delta \phi_{r,\mathrm{IF}}^{\bar{s}}(k)$ are present. Their time-averaged version are reserved for the estimable phase biases $\bar{\tilde{\delta}}_{,\mathrm{IF}}^{\bar{s}}$. As a result, only their time differences

$$
\begin{aligned}
\mathsf{E}(\Delta \phi_{r,\mathrm{IF}}^{\bar{s}}(k) - \Delta \phi_{r,\mathrm{IF}}^{\bar{s}}(k-1)) &= (d\tilde{t}_r(k) - d\tilde{t}^{\bar{s}}(k)) \\
&\quad - (d\tilde{t}_r(k-1) - d\tilde{t}^{\bar{s}}(k-1))
\end{aligned}
\tag{10}
$$

contribute to the clock solutions. Substitution of the equalities $d\hat{\tilde{t}}_r(i) - d\hat{\tilde{t}}^{\bar{s}}(i) = \Delta p_{r,\mathrm{IF}}^{\bar{s}}(i)$ ($i = k - 1, k$) into the preceding equation gives the condition equation

$$
\begin{aligned}
\mathsf{E}(\{\Delta \phi_{r,\mathrm{IF}}^{\bar{s}}(k) - \Delta \phi_{r,\mathrm{IF}}^{\bar{s}}(k-1)\} \\
- \{\Delta p_{r,\mathrm{IF}}^{\bar{s}}(k) - \Delta p_{r,\mathrm{IF}}^{\bar{s}}(k-1)\}) = 0
\end{aligned}
\tag{11}
$$

The misclosure, formed by the above condition equations is, however, uncorrelated with the process noises $n_{dt^{\bar{s}}}(i)$ ($i = 3, \ldots, k$), thus not stopping the variance increase of the solution $d\hat{\tilde{t}}^{\bar{s}}(k)$. One concludes, therefore, that it is the variance increase of the satellite-averaged component $d\hat{\tilde{t}}^{\bar{s}}(k)$

that leads to variance increase of both the estimable satellite and receiver clock solutions $d\hat{\tilde{t}}^{\bar{s}}(k)$ and $d\hat{\tilde{t}}_r(k)$, respectively.

The dependency of the solutions of the estimable clock parameters on the satellite-averaged component $d\hat{\tilde{t}}^{\bar{s}}(k)$ has another consequence. Since the interpretation of the average $d\tilde{t}^{\bar{s}}(k)$ changes if the number of tracked satellites changes, one would expect to observe a change in the clock solutions upon tracking new satellites. Figures 1 and 2 only show time-series of the receiver clock estimation error over the first 900 epochs where no newly tracked satellites are present. To show the role of such satellites on the clock estimation error, we extend the time span of the time series to 3600 epochs in Fig. 3, left panel. As shown, the presence of newly tracked satellites causes jumps in the receiver clock estimates as well as in their error variances around epochs 900 and 1800. As soon as a new satellite is involved in the processing, the provider filter needs to account for the estimation of the new unknown parameters corresponding to the satellite, changing the solution $d\hat{\tilde{t}}^{\bar{s}}(k)$, thereby causing an increase in the variance of the clock solutions.

Let us assume now that the correction provider has its GNSS receiver connected to a more stable external clock, e.g., a high-quality hydrogen maser clock. In this case, one can do away with the assumption of a highly time-varying clock and model its temporal behavior with a constant-velocity setup similar to that of the satellite clocks. Table 1 also presents the additional estimable parameters that occur by switching from a time-unlinked to a time-linked receiver clock under a constant-velocity setup. As shown, the inclusion of a receiver clock dynamic model does not change the parameters' estimability, but just introduces an extra unknown parameter, i.e., the estimable receiver clock velocities $\partial d\tilde{t}_r(k)$. Similar to the satellite clock velocities in Table 1, the original receiver counterparts are also biased by the receiver clock term. Therefore, in this setup, one can exploit the temporal stability provided by the external atomic clock and determine more precise solutions of the receiver clock that can serve in timing applications. As will be shown later on, though, care must be exercised to correctly interpret the determined clock solutions and their quality information.

Now the question is whether the solution's behavior of the receiver clock remains invariant under the assumption of having an ultra-stable receiver clock, i.e., one that can be linked in time based on a constant-velocity setup. The right panel of Fig. 3 depicts the estimated receiver clock error and its confidence intervals for system noise STD equal to 0.1 mm/$\sqrt{s^3}$. One can observe that the more stringent the system noise characteristics are, the tighter the confidence intervals become. When it comes to the receiver clock error itself, no direct comparison can be done as the two solutions comprise different realizations of $d\tilde{t}_r$, even though one would expect that the divergence becomes smaller with a decreased

Fig. 3 Time-series of the receiver clock estimation error (solid line) and its 99.9% confidence interval (dashed lines) without a dynamic model (left) and with a constant-velocity model (right) for the temporal behavior of the receiver clock. The acceleration system noise STD used in the latter case is 0.1 mm/$\sqrt{s^3}$
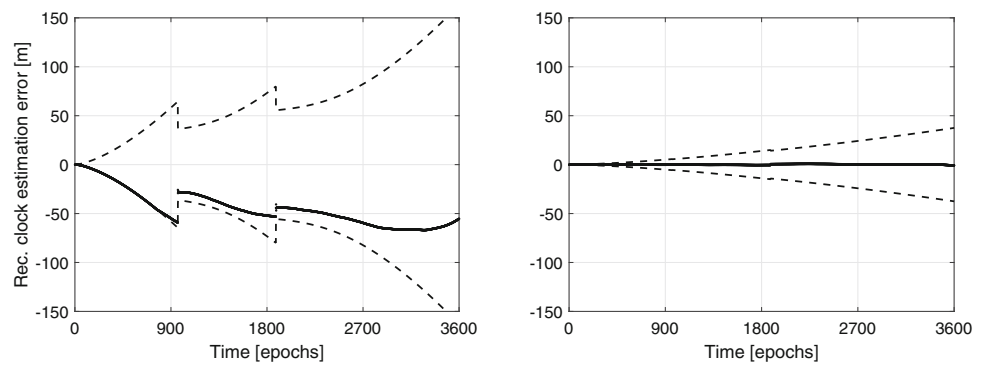

Fig. 4 Time-series of the satellite clock estimation errors (colored dots) and their 99.9% confidence intervals (black dashed lines) under two different $\mathcal{S}$-system choices: the receiver clock is minimum-constrained as $\mathcal{S}$-basis, i.e., only at the first two epochs (*top*) and constrained as $\mathcal{S}$-basis at every processing epoch (*bottom*). *Left*: Undifferenced clocks. *Right*: Between-satellite single-differenced clocks. A constant-velocity setup has been used to model the temporal behavior of the satellite clocks. The confidence intervals refer to the clock of a representative satellite that is tracked since the provider-filter initialization. Each color represents a different GPS satellite
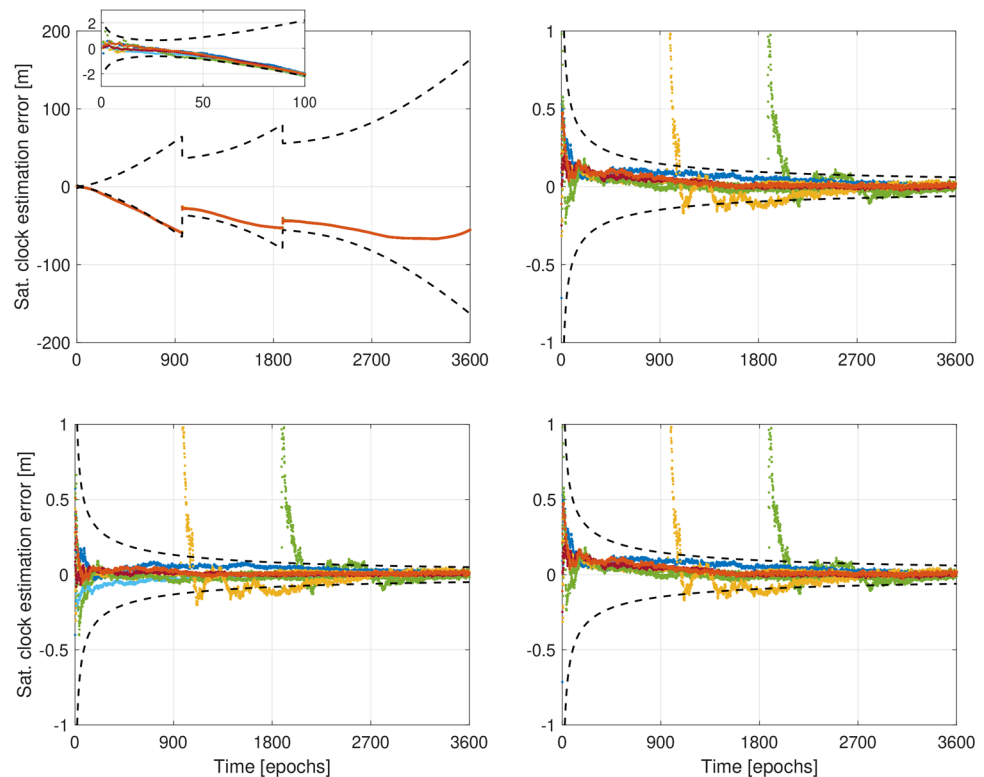
system noise variance. In addition, the magnitude of the introduced jumps because of newly arrived satellites seems to go in accordance with the clock system noise variance. The reason lies in the fact that a smaller system noise variance implies that more confidence is placed on the dynamic model rather than the introduced measurements at every epoch.

It should be remarked that the above results were obtained using a forward-only Kalman filter which is often utilized in real-time applications. In a post-processing exercise where one is able to perform a forward–backward filter approach, the error variance of the smoothed receiver clock estimates would never be larger than that of the forward-only-based estimates.

3.1.2 Individual corrections

Satellite clocks

The first subset of the positioning corrections to aid the PPP-RTK user consists of the estimable satellite clocks. In our simulation setup, the single-station provider data processing resulted in the satellite clock errors and their STDs shown at the top-left panel of Fig. 4, which includes the state errors for all observed GPS satellites during the processed one hour. Note that these results refer to the undifferenced version of the clocks. One can immediately observe that the satellite clock results fully resemble those shown for the receiver clock (cf. Fig. 1) and are consistent for all observed GPS satellites. The question is now whether the component of the satellite clocks, contributing to user positioning, can be pre-

cisely determined in a constant-velocity setup. As we will see in the following, the answer is affirmative.

In the attempt to evaluate the quality of the estimated satellite clocks, one may be inclined to defy the usage of a single-station provider to determine the estimable satellite clocks, due to the nonzero-mean state errors and their increasing variances over time. As shown by (9), the variance of the satellite-averaged satellite clock will experience an increase over time as a result of its accumulated system noise. One should also study the variance behavior of its satellite-differenced component in order to fully characterize the variance behavior of the satellite clocks.

Considering now that *there exists* redundancy in the system of satellite-differenced IF code observations from the third epoch onwards, due to the absence of the receiver clock, one can infer that the multi-epoch satellite-differenced clocks will experience a precision improvement over time. Combined with our finding in Sect. 3.1.1, it becomes clear that the variance behavior of the satellite clocks $d\tilde{t}^s$ will be dominated by the variance-increase of their satellite-averaged counterparts. These conclusions can be graphically demonstrated in Fig. 4. At the top-right panel of the figure, one can observe that the single-differenced satellite clocks become *indeed* more precise over time and converge to their true values. The effectiveness of the between-satellite single-differenced PPP-RTK corrections on the user level has also been discussed in Khodabandeh and Teunissen (2015). As with the receiver clock solution, it is the increase in the solutions' variance over time that increases the probability that the undifferenced satellite clock estimation errors diverge from their expected value (i.e., zero). In case the provider makes use of an $\mathcal{S}$-basis that includes the receiver clock $dt_r(i)$ *at every epoch*, as is usually the case in the analysis centers of the International GNSS Service (Steigenberger et al. 2015), one would end up with the undifferenced and satellite-differenced satellite clock estimation errors at the bottom-left and bottom-right panels, respectively, of Fig. 4.

At this point, one may still wonder whether these *seemingly imprecise* undifferenced satellite clock estimates can *actually* be utilized by the PPP-RTK positioning users to achieve centimeter-level positioning. The fact that the user receiver clock is assumed to be unlinked in time allows us to reasonably expect the increasing error variance of the satellite clocks, due to their satellite-averaged version, to be mapped to the user receiver clock. This practically means that the *seemingly imprecise* satellite clock estimates do not impact the user ambiguity and position parameters, leaving ambiguity-fixed positioning unaffected.

Now consider the case in which the user employs a dynamic model for his receiver clock parameter, e.g., a constant-velocity setup, for which the system noise of the receiver clock velocity is known. Although one would expect in such a setup to obtain improved performance for his

receiver clock, e.g., for timing applications, this would not be true given the satellite clock corrections $d\hat{\tilde{t}}^s(k)$. This is due to the fact that the latter are lumped with the parameter $[k-1]\Delta t \partial d\bar{t}_r$ (cf. Table 1), which was introduced after assigning a constant-velocity setup for the satellite clocks. Consequently, the behavior of the user's receiver clock, regardless if its temporal behavior is modeled by the user through the user's dynamic model, will also be governed by the single-station provider's satellite clock corrections.

Satellite phase biases

We now turn our attention to the key correction component needed for recovering the integerness of user ambiguities and, therefore, achieving single-receiver integer ambiguity resolution, namely the *satellite phase biases*. The resulting L1 satellite phase bias errors and their STDs, as estimated in our simulated single-station setup, are depicted in Fig. 5. After convergence, the satellite phase bias estimation errors approach the zero value and are shown to completely lie within the confidence interval. Instead of showing the satellite phase biases for L2 as well, the figure shows their difference, namely the wide-lane (WL) satellite phase biases, i.e., $\hat{\bar{\delta}}^s_{,\mathrm{WL}} = \hat{\bar{\delta}}^s_{,1} - \hat{\bar{\delta}}^s_{,2}$. The WL biases are more precise than their uncombined counterparts due to the high correlation between the latter, with a 30-fold precision improvement after convergence.

In providing phase bias estimates to the user, one may opt for either the originally estimated states $\hat{\bar{\delta}}^s_{,j}$ or their fractional part $\mathrm{frac}(\hat{\bar{\delta}}^s_{,j})$, as is the case in the fractional cycle bias (FCB) model (Ge et al. 2008). The fractional operator is defined as $\mathrm{frac}(x) = x - \lfloor x \rceil$, where the symbol $\lfloor x \rceil$ denotes rounding to the nearest integer of x. Ideally, when there is no 'randomness' involved in $\lfloor x \rceil$, the integer shifting $x - \lfloor x \rceil$ would not impact the distribution of x other than its location. In that case, application of the fractional operator to the phase bias solutions maintains the integerness of the user ambiguities. However, the phase bias solutions and their integer-rounding estimators are functions of the random GNSS measurements. Consequently, the distributional properties of the phase bias solutions will be affected by the fractional operator due to the non-integer mean of the phase biases, the larger the level of randomness becomes in the integer-rounding estimator $\lfloor x \rceil$. For instance, consider Fig. 6 in which the histograms of the L1 and WL satellite phase bias estimation errors, together with their fractional versions, are depicted for a representative satellite using 100 observable samples. In the case of WL phase biases, the fractional estimator exhibits estimation errors almost the same as those of the original WL phase bias estimator. This is due to the rather high precision of the WL phase bias solutions. In the case of L1 phase biases, however, the estimation errors of the fractional estimator fail to be symmetric around zero, indicating that the fractional estimator
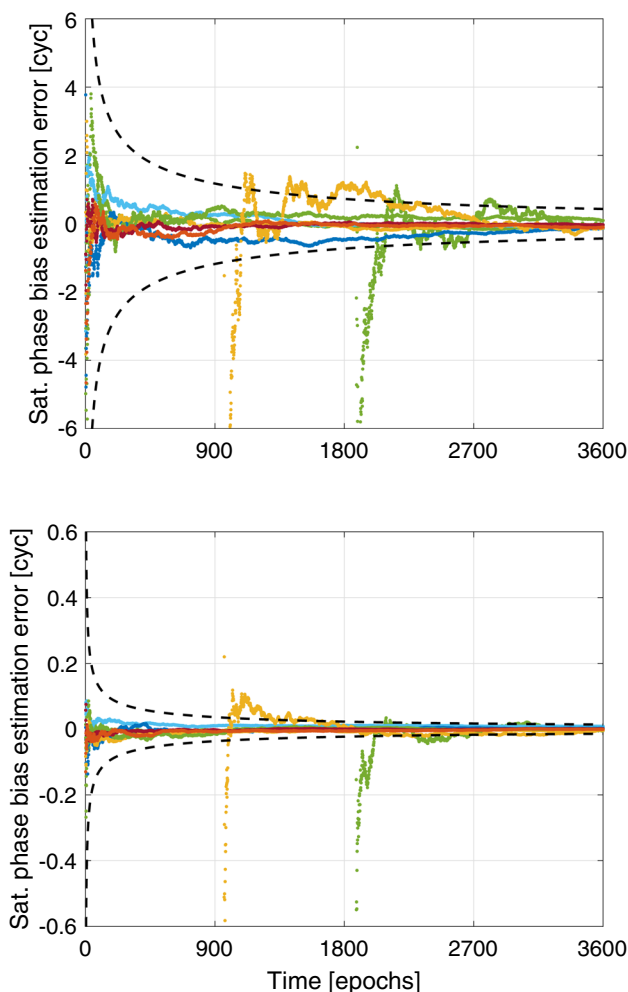
Fig. 5 Time-series of the L1 (top) and WL (bottom) satellite phase bias estimation errors (colored dots) and their 99.9% confidence intervals (black dashed lines). The confidence intervals refer to the phase bias of a representative satellite that is tracked since the provider-filter initialization. Each color represents a different GPS satellite

Fig. 6 Histograms of the L1 (top) and WL (bottom) phase biases in their original (green) and fractional (blue) versions, along with the formal PDF (red) of the original phase biases, based on independent Kalman filter realizations of 100 normally-distributed observable samples. The dark-green color occurs due to the full or partial overlap of the two histograms. The results correspond to the estimated L1 and WL phase biases of an individual GPS satellite at 3600 s since the provider-filter initialization

delivers non-Gaussian-distributed phase bias solutions. This illustrative example highlights the serious pitfall that exists when delivering the fractional version of the phase biases to the users and underlines the importance of exercising proper care in the evaluation of statistics for the user-corrected phase measurements, see also (Teunissen and Khodabandeh 2015).

3.1.3 Combined corrections

The analysis of the individual corrections is useful if one wants to study the temporal characteristics and estimation quality of the individual parameters. However, when the user ambiguity-resolved positioning performance is concerned, our earlier contributions show that such a quality judgment disguises key information, resulting in serious pitfalls (Khodabandeh and Teunissen 2015; Psychas et al.
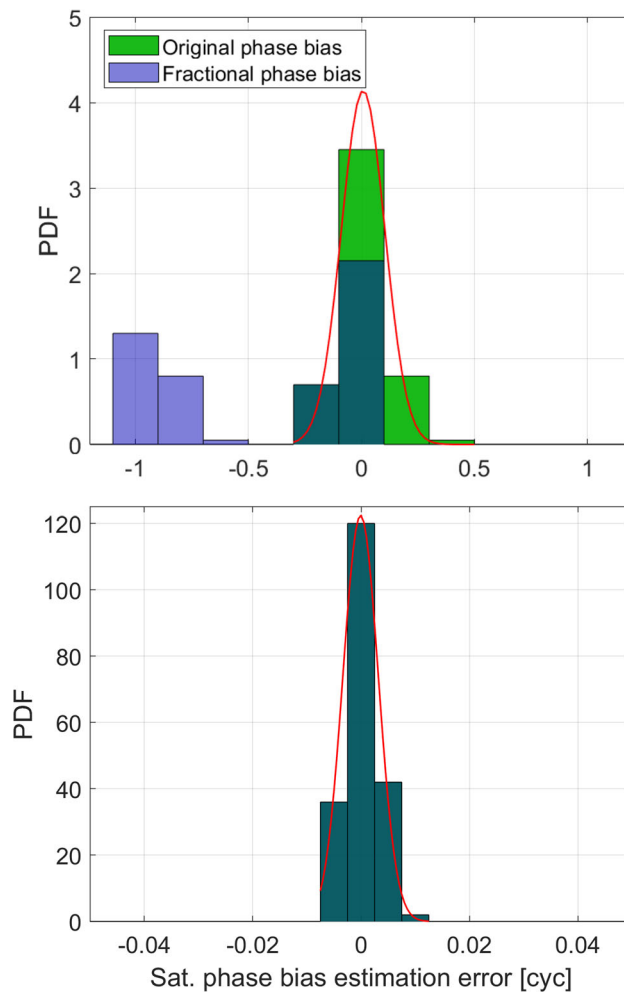
2022). What matters is their combined effect, revealing the role of high correlation that exists between the individual corrections. The combined phase and code corrections $\hat{c}^s_{\phi,j}(k)$ and $\hat{c}^s_{p,j}(k)$ are, respectively, given by

$$\begin{bmatrix} \hat{c}^s_{\phi,j}(k) \\ \hat{c}^s_{p,j}(k) \end{bmatrix} = \begin{bmatrix} d\hat{\tilde{t}}^s(k) + \mu_j \hat{\tilde{t}}^s_r(k) + \lambda_j \hat{\tilde{\delta}}^s_{,j}(k) \\ d\hat{\tilde{t}}^s(k) - \mu_j \hat{\tilde{t}}^s_r(k) + \hat{\tilde{d}}^s_{,j}(k) \end{bmatrix} \quad (12)$$

That both the code and phase PPP-RTK corrections contain the satellite clock and ionospheric delay estimates implies the presence of correlation between them, a property that may often be overlooked in positioning applications. Whether this correlation remains constant or to what extent it increases as a function of latency remains a topic of analy-

Fig. 7 Formal STDs of the between-satellite combined PPP-RTK code (top-left) and phase (top-right) corrections, along with the code/phase correlation (bottom), as a function of time and correction latency. The results correspond to an individual GPS satellite
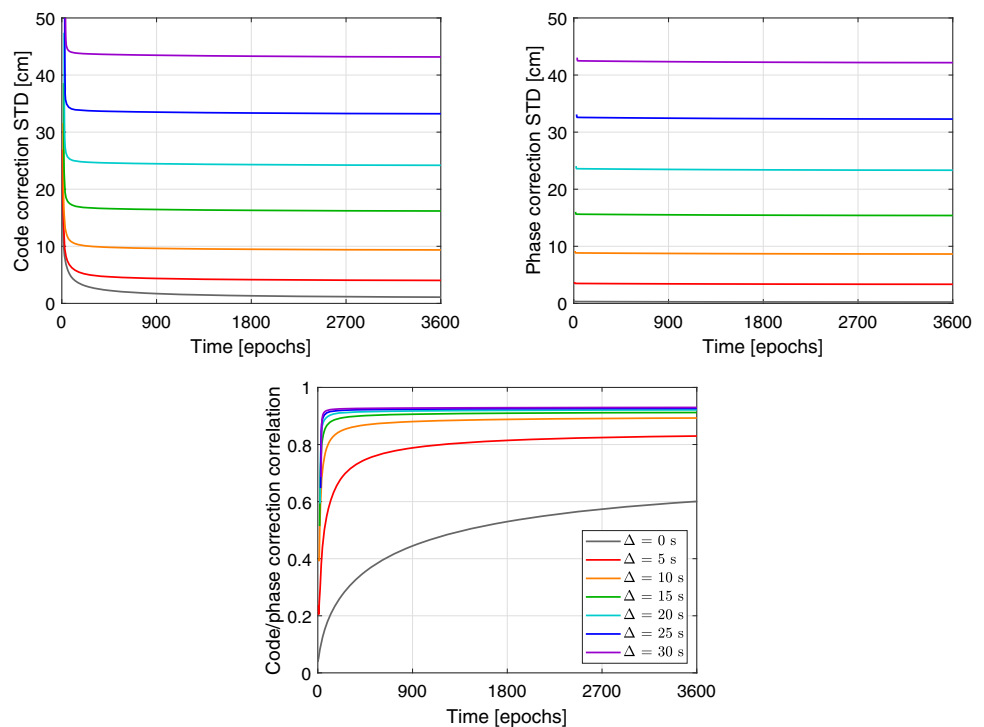
sis in this subsection. Figure 7 shows the formal STD of the PPP-RTK code and phase combined corrections of a representative satellite, as well as the correlation between them, in their satellite-differenced version. Since the undifferenced corrections experience a variance increase due to the variance increase of the estimable satellite clocks, we do not present the formal STDs of the undifferenced corrections for brevity. To highlight the role played by the correction latency, we also compute these formal measures for nonzero latencies up to 30 s with a time-prediction step as in Khodabandeh et al. (2023). In the case of an instantaneous delivery of the corrections to the users, i.e., without any time delay, the satellite-differenced PPP-RTK code and phase correctional uncertainties lie in the few cm and mm levels, while one can observe one order of magnitude increase for a latency of 30 s. The code-phase correction correlation with a zero latency shown at the bottom row of the figure shows an increase over time, which is due to the increasing precision of the combined corrections over time, the rate of which was found to be higher compared to the one of the almost time-invariant code-phase correction covariance. When latency is introduced between the correction generation and their application at the user side, it can be seen that the correlation increases with increasing latency. This is attributed to the uncertainty amplification that takes place in the corrections' time-prediction step. After the steady state has been achieved, the correlation values reach the 0.6−0.9 level, indicating that they are non-negligible contributors to the user stochastic model.

3.1.4 Time correlation

We have so far focused on the correctional uncertainty that has been shown to get amplified in the presence of nonzero latencies and, as such, rigorous parameter estimation at the PPP-RTK user level needs to consider such uncertainty. Another interesting property of the multi-epoch positioning corrections that is often overlooked or ignored is their time correlation. It is reminded here that the multi-epoch filtered corrections are inherently correlated in time. The reason behind neglecting such a property is of twofold nature. First, the autocorrelation of the multi-epoch filtered corrections is reasonably assumed to vanish over considerable time spans. Second, the realization of multi-epoch recursive estimators, such as the Kalman filter, relies on diagonal weight matrices and, as a result, the presence of nonzero time correlation in the filtered corrections and subsequently to the user-corrected data leads to a misspecified user filter that delivers sub-optimal results in the minimum-variance sense. In obtaining rigorous parameter estimation based on multiple epochs of data, one should take recourse to multi-epoch batch estimators that are not favorable in real-time applications.

To better understand the results presented in the following, we present here how fast the temporal correlation of the PPP-RTK combined corrections decays over time. Figure 8 depicts the temporal correlation of the satellite-differenced PPP-RTK code corrections for latencies ranging from 0 to 30 s. Since similar behavior between the temporal correlation of the code and phase corrections was observed, we do
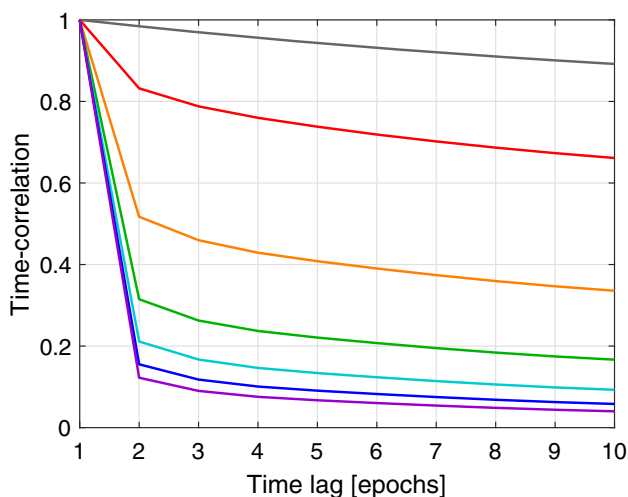
Fig. 8 Time correlation of the estimated between-satellite combined PPP-RTK code corrections as function of time lag with a latency ranging from 0 to 30 s. The results correspond to an individual GPS satellite. The legend of Fig. 7 is applicable here

not present the time-series of the latter for brevity. One immediately observes that, regardless of the latency applied, the correlation decays over time with the rate of decrease becoming more pronounced the longer the latency is. As a result, the assumption of a vanishing temporal correlation is plausible, with its minimum being brought only after a certain number of epochs. Whether neglecting the time correlation of the user-corrected measurements has an impact or not on the expected user performance is left to be investigated in the following section.

4 User impact

As the goal of PPP-RTK is in principle to enable single-receiver user integer ambiguity resolution aiming to obtain centimeter-level positioning, we will, in this section, present and analyze the impact the precision, time correlation and latency of the corrections have on the quality description of the user position and ambiguity solutions, as that would be observed from the provider. We perform this analysis for both the single-epoch and multi-epoch user setups. The distance between the provider and user receivers is assumed to be short enough so that they both experience the same atmospheric delays and have approximately equal line-of-sight unit vectors.

4.1 Single-epoch setup

To show how the user parameter solutions are impacted by the combined corrections (12), we make use of their vectorial forms. Accordingly, the vector of corrections at

epoch k is defined as $\hat{c}_k = [\hat{c}^s_{\phi,1}(k), \hat{c}^s_{p,1}(k), \ldots, \hat{c}^s_{\phi,j}(k),$ $\hat{c}^s_{p,j}(k), \ldots, \hat{c}^s_{\phi,f}(k), \hat{c}^s_{p,f}(k)]$ for $s = 1, \ldots, m$ and $j = 1, \ldots, f$. Adding this vector to the user observation vector at epoch k, say y_k, gives the user observation equations in their linearized form as follows

$$E(y_k + \hat{c}_k) = A_k\, x_k \tag{13}$$

where the user unknown parameter vector x_k is linked to the *corrected* observation vector $(y_k + \hat{c}_k)$ through the full-rank design matrix A_k.

We now analyze the single-epoch user ambiguity resolution and positioning performances as functions of correction latency. Judging from the results shown in the previous section, one can expect both the ambiguity resolution and the positioning performance to be largely driven from the uncertainty of the corrections and the latency the latter are provided with. Assuming the user correctly specifies his stochastic model, he performs a best estimation in the minimum-variance sense:

$$Q_{\hat{x}_k} = A_k^+ Q_{\tilde{y}_k} A_k^{+T}, \quad A_k^+ = (A_k^T Q_{\tilde{y}_k}^{-1} A_k)^{-1} A_k^T Q_{\tilde{y}_k}^{-1} \tag{14}$$

where $Q_{\tilde{y}_k} = Q_{y_k} + Q_{\hat{c}_k}$ is the variance matrix of the corrected observation vector $(y_k + \hat{c}_k)$. The user data variance matrix is evaluated as $Q_{y_k} = \text{blkdiag}(C_{\phi\phi}, C_{pp}) \otimes W_k^{-1}$, with $\otimes$ being the Kronecker matrix product. The matrices $C_{\phi\phi}$ and C_{pp} are the covariance matrices of the phase and code observables, respectively, at zenith. The zenith-referenced STDs of the user phase and code data have been set to 3 mm and 30 cm, respectively, assuming that the user receiver provides measurements of lower quality compared to those of the provider receiver. The $m \times m$ matrix $W_k = \text{diag}(w_k^1, \ldots, w_k^m)$ contains the elevation dependent weights of the satellites tracked by the user at epoch k.

To provide insight into the user performance, we evaluated the user Ambiguity Dilution Of Precision (ADOP; Teunissen 1997), as the geometric average of the sequential conditional STDs of ambiguities, and ambiguity-float and ambiguity-fixed positioning precision as shown in Fig. 9. Note that, since ambiguity resolution may have different responses to various functions of the position parameters, we have employed the square root of the position variance matrix' determinant taken to the power one over three, which represents the average positioning precision.

Starting with the instantaneous minimum-variance user solutions at the top panel of Fig. 9, one can clearly observe how the user ADOP is driven by the correction latency, with a 30 s time delay bringing it to an ADOP ranging from 0.5 to 0.6 cycles. As a rule of thumb, ADOP values smaller than about 0.12 cycle correspond with success rates larger than 0.999 (Odijk and Teunissen 2008). The increase in the ADOP values stems from the fact that, given that the user phase data are
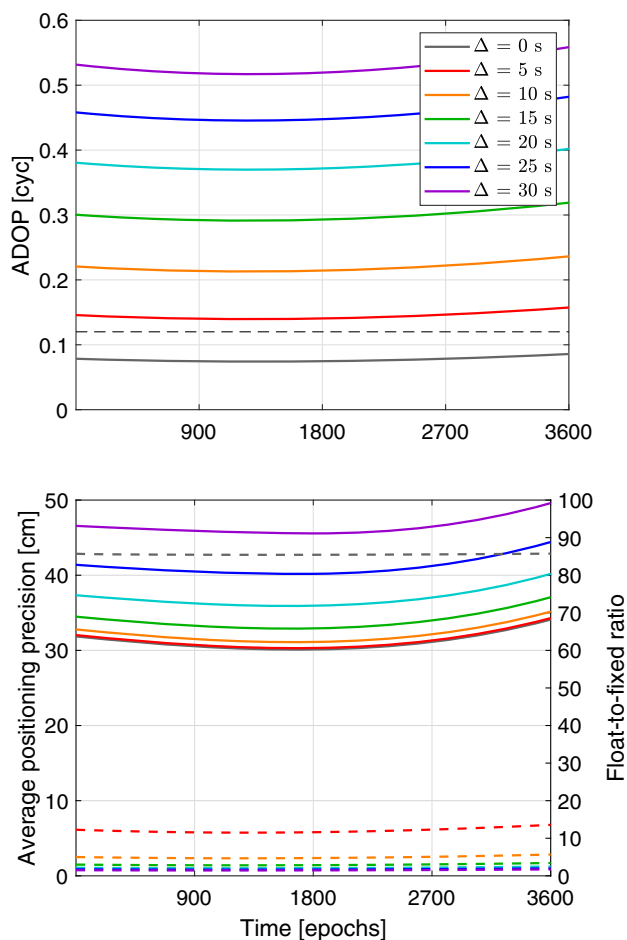
Fig. 9 GPS L1/L2 single-epoch user ADOP (top) and geometric mean of the float position conditional STDs (bottom; solid lines) with their float-to-fixed ratios (bottom; dashed lines) as a function of latency when considering the correct user-measurement variance matrix. The horizontal dashed line in the top-panel denotes the value of 0.12 cycles

reserved for the phase ambiguities and thus for the resulting ADOP, the combined phase corrections become less precise than the phase data with increasing latency (cf. Fig. 7). As for the float average positioning precision, no considerable impact can be seen unless larger latencies are used. This is in fact expected, since the code data, which are less precise than the combined code corrections for larger time delays (cf. Fig. 7), drives the float position estimates in a single-epoch user setup. Assuming now that the phase ambiguities can be correctly fixed, the dashed lines in the bottom panel of the figure show how many times the precision of the ambiguity-float position solutions improves. Since in this case it is the user phase data that govern the fixed position precision, one would expect an about two orders of magnitude precision

improvement, which is actually not the case except for the zero-latency case. This is due to the fact that the phase data are affected by the uncertainty of time-predicted PPP-RTK corrections, thereby limiting the range of improvement.

4.2 Multi-epoch setup

So far we based our analysis on the single-epoch user setup, where data at each epoch are processed independently to produce epoch-by-epoch user parameter estimates, and for which promising results have been demonstrated for instantaneous user ambiguity resolution and positioning even for high latencies (Khodabandeh 2021; Psychas et al. 2022). One may also opt for a multi-epoch processing exploiting the time stability of the phase ambiguities in a dynamic model using either a Kalman filter (Kalman 1960) or its generalized version with a relaxed dynamic model that involves only a subset of the state vector (Teunissen et al. 2021). Once a (generalized) Kalman filter is employed by the user, the ambiguity-float user parameter solutions will get more precise over time due to an implicit accumulation of data over epochs.

In this case, one would want to ensure that the filter's underlying stochastic assumptions are valid for the execution of a rigorous multi-epoch processing. However, the application of the multi-epoch filtered corrections to the normally distributed user data violates one of the Kalman filter measurement model's assumptions in that the user-measurement noise ceases to be uncorrelated in time. The reason lies in the fact that the single-station provider processed the code and phase measurements in a Kalman filter and, as such, the determined corrections are inherently correlated in time. To circumvent this limitation, Khodabandeh et al. (2023) proposed a new multi-epoch formulation of the PPP-RTK user filter that can outperform its commonly used counterpart and deliver close-to-minimum-variance solutions.

In practice, the PPP-RTK corrections are often treated as nonrandom (deterministic) quantities, mainly due to the excessive amount of quality description information that needs to be transmitted to the user (Odijk et al. 2014), thereby neglecting both their uncertainty and their temporal correlation. Since the existing user filter formulations become misspecified and provide an incorrect or sub-optimal quality description, we determine and analyze the user-optimal expected performance using a batch formulation of the Kalman filter, which considers both the uncertainty and time correlation of the provided corrections. In carrying out this analysis, we form the user-measurement variance matrix as follows:
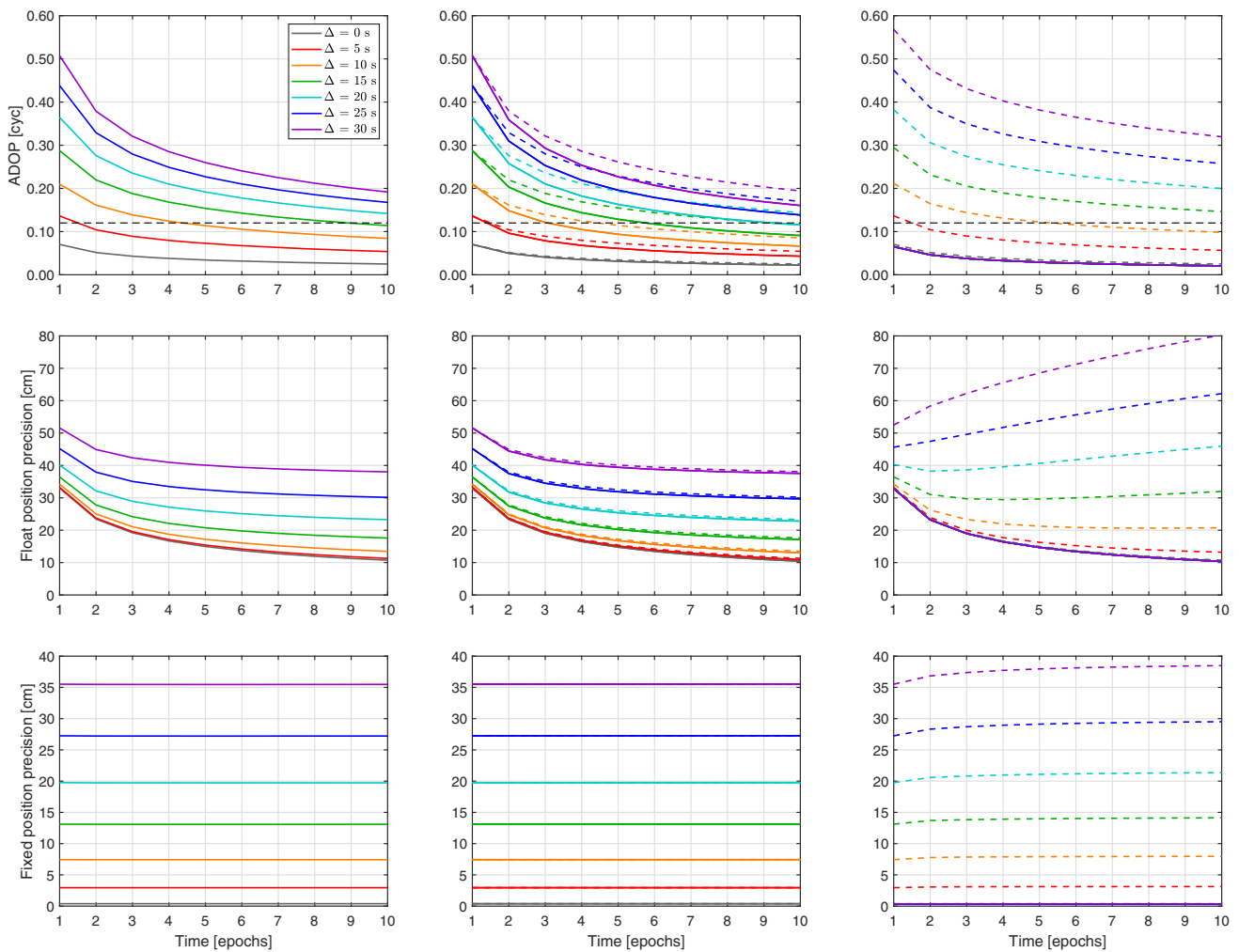
Fig. 10 GPS L1/L2 multi-epoch user ADOP (top row) and average positioning precision with float (middle row) and fixed (bottom row) ambiguities for 10 epochs of data as a function of correction latency. The figures in the first column refer to the optimal minimum-variance solution where the user considers the correctional uncertainty and time correlation (*Case 1*). The second column figures refer to the sub-optimal solution where the user considers only the correctional uncertainty, thus neglecting the time correlation (*Case 2*). The third column figures refer to the often computed solution where the user ignores the correctional uncertainty and time correlation (*Case 3*). The solid and dashed lines represent the reported and actual formal measures, with the latter being estimated based on correct variance propagation. The correction generation starting time is 09:25:00, while the user parameter estimation begins at 09:26:00

$$\mathsf{D}\begin{pmatrix} y_k + \hat{c}_{k|k-\tau} \\ \vdots \\ y_{k+K} + \hat{c}_{k+K|k+K-\tau} \end{pmatrix} = \mathrm{diag}(Q_{y_k}, \ldots, Q_{y_{k+K}})$$

$$+ \begin{bmatrix} Q_{\hat{c}_{k|k-\tau}} & \cdots & Q_{\hat{c}_{k|k-\tau}, \hat{c}_{k+K|k+K-\tau}} \\ \vdots & \ddots & \vdots \\ Q^{\mathrm{T}}_{\hat{c}_{k|k-\tau}, \hat{c}_{k+K|k+K-\tau}} & \cdots & Q_{\hat{c}_{k+K|k+K-\tau}} \end{bmatrix}$$

(15)

The user position and receiver clock parameters are assumed to be unlinked in time, while the remaining parameters are treated as time-constant parameters.

To gain an insight into the impact that neglecting the correction uncertainty and time correlation has on the user parameter precision description, the formal measures describing the ambiguity resolution strength and positioning quality are visualized and analyzed below. Shown in Fig. 10 are the time-series of the user ADOP (top row) and the average positioning precision with float (middle row) and fixed (bottom row) ambiguities for batches up to 10 epochs of data and for correction latencies up to 30 s. We consider here three

distinct cases regarding the error variance-matrix of the time-predicted PPP-RTK corrections that the user makes use of:

- *Case 1* considering both the uncertainty and the time correlation of the corrections (left column), which results in the minimum-variance solutions
- *Case 2* considering only the uncertainty of the corrections (middle column)
- *Case 3* neglecting both the uncertainty and the time correlation of the corrections (right column), which is the strategy often adopted in practice

Note that in the presence of a misspecified stochastic model, i.e., Cases 2 and 3 (middle and right columns), the *actual* formal measures are evaluated with a correct variance propagation and are shown in the figure with dashed lines, while the reported counterparts with solid lines.

Let us first focus on Case 1, where the user has access to the complete characterization of the correctional stochastic information and can obtain optimal solutions in the minimum-variance sense. In the left-column panels of Fig. 10, one can observe that the ADOP and ambiguity-float position standard deviation decrease over time, but get amplified in the presence of nonzero latencies. The first finding is due to the accumulation of multiple epochs of data that strengthens the underlying user model, thereby leading to more precise parameter solutions, while the second one is also expected since the user-corrected data are affected by the uncertainty of the corrections that increase as the latency gets higher. When it comes to the ambiguity-fixed results (bottom row), the sensitivity of the positioning precision description to the correction latency is evident as a result of the fact that the phase data are affected by the amplified correctional uncertainty. However, the ambiguity-fixed position standard deviations are shown not to be sensitive to the number of epochs as the former are only function of the ambiguity-fixed phase data uncertainty. Notable is the fact that the ambiguity-fixed precision under a 30 s correction latency is about 35 cm compared to the 4 mm level achieved with instantaneously delivered corrections.

When the PPP-RTK user neglects or has no access to the time correlation of the corrections (Case 2), the reported ADOP values shown in the middle column of Fig. 10 get falsely smaller than the minimum-variance counterparts, and the difference with the actual formal measures becomes more evident the higher the latency becomes. This is not the case, though, with the position standard deviations that show negligible changes for both float and fixed solutions. This practically indicates that, from a quality description point of view, neglecting the correctional time correlation does not significantly impact the average positioning precision, which almost mimics the one of the minimum-variance solution. The close agreement between the Case 2 and close-to-minimum-variance solutions has also been reported in Khodabandeh et al. (2023).

Shown at the right column of Fig. 10 are the results of Case 3, i.e., when the user is not provided with or neglects both the corrections' uncertainty and time correlation. One can then observe that, regardless of the correction latency, the *reported* ADOP and positioning precision exhibit the same high level of performance. However, we recall here that these results reflect the *assumed* user performance, which describe a misleading and incorrect quality description. Given that the correction provider has access to the full correction uncertainty information, a correct variance propagation leads to the *actual* user performance that is in fact achieved by the user. Observing the rightmost panels, one can notice the considerable gap between the actual and incorrect formal ambiguity resolution and positioning quality description that becomes more pronounced with increasing correction latency. As an example, note that with 10 epochs of data the user is misled as he is provided with an ADOP of 0.02 cycles and an ambiguity-fixed positioning precision of about 3 mm, indicating successful ambiguity-resolved solutions, while in fact the actual measures are 0.32 cycles and 38 cm, respectively. This implies that neglecting both of these stochastic contributions has an adverse impact on the user performance as it leads to incorrect and over-optimistic quality description of the user parameter solutions.

5 Summary and conclusions

In this contribution, we studied and presented the intricacies inherent in *multi-epoch filtered* PPP-RTK corrections that aid users in realizing single-receiver integer ambiguity-resolved positioning and, thus, require a careful examination. Although one is able to analytically infer the statistical properties of their estimable parameter solutions, it was shown that one can be in fact misled by analyzing solely their characteristics and behavior over time. To highlight the pitfalls and effectively identify their root causes, we developed a simulation platform that allows one to have full control over the properties under investigation. Our main findings are summarized as follows:

- *Misleading impressions through single realizations.* We started off by discussing how a single realization of the estimable clock parameter solutions can be misleading due to the nonzero-mean estimation error time-series one could be confronted with. It was highlighted that multi-epoch parameter solutions are *random processes*, while the Kalman filter only delivers a sample out of their infinitely many *realizations*. After accumulating multiple independent Kalman filter realizations, we demonstrated

that the unbiasedness property of the estimable parameters holds.

- *Variance-increase of clocks.* The divergence of the clock estimation errors from the expected zero value over time was also reflected on the formal confidence intervals of their estimable forms. In explaining this phenomenal behavior, analytical expressions were presented showing that the contributing factor to such a behavior is the solution's variance of the satellite-averaged component of the undifferenced satellite clocks as a result of accumulated system noise and the absence of redundancy. It was shown that the satellite-differenced clocks, being the ones that take an active role for user positioning, become more precise over time due to the presence of redundancy in the satellite-differenced system of observation equations.

- *The fractional estimator delivers non-Gaussian-distributed solutions.* The widely used FCB model for PPP-RTK was evaluated as to whether the fractional estimator can deliver proper phase bias solutions, for which the level of randomness involved in the integer-rounding estimator plays a decisive role. By means of an illustrative example, we demonstrated that the application of the fractional operator on the Gaussian-distributed frequency-specific satellite phase bias solutions can alter their distributional properties, thereby delivering non-Gaussian-distributed phase bias solutions to the users and subsequently affecting the distribution of the user float ambiguities.

- *Role of the correction latency and time correlation.* Since it is the combined form of the PPP-RTK corrections that matters for user positioning, their sensitivity to the latency was analyzed. It was shown that the larger the latency, the larger the combined correctional uncertainty and the code/phase correctional correlation become. On the contrary, the time correlation underlying the multi-epoch filtered corrections experienced a reduction over time, especially in the presence of large latencies, indicating that the assumption of a rapidly vanishing temporal correlation employed in user positioning setups is plausible.

- *Sub-optimal user performance.* Supported by the numerical results, our analysis showed that the reported quality description of the user ambiguity resolution and positioning performance, as that would be observed from a provider, can be misleading and incorrect upon ignoring the correctional uncertainty, with the effect being more pronounced for larger latencies. Neglecting only the time correlation information, though, exhibited only slight deviations between the user-reported and user-actual ADOP, while the positioning precision was shown to resemble the one achieved in the minimum-variance solution. Addressing the extent to which the user performance may be further affected by neglecting other parts of the corrections' stochastic information, such as the between-satellite correctional covariance, is a topic of future work.

References

Collins P (2008) Isolating and estimating undifferenced GPS integer ambiguities. In: Proceedings of the 2008 National Technical Meeting of the Institute of Navigation, San Diego, pp 720–732

Duong V, Harima K, Choy S, Laurichesse D, Rizos C (2019) Assessing the performance of multi-frequency GPS, Galileo and BeiDou PPP ambiguity resolution. J Spat Sci. https://doi.org/10.1080/14498596.2019.1658652

Ge M, Gendt G, Rothacher M, Shi C, Liu J (2008) Resolution of GPS carrier-phase ambiguities in Precise Point Positioning (PPP) with daily observations. J Geod 82(7):389–399. https://doi.org/10.1007/s00190-007-0187-4

Geng J, Shi C, Ge M, Dodson AH, Lou Y, Zhao Q, Liu J (2012) Improving the estimation of fractional-cycle biases for ambiguity resolution in precise point positioning. J Geod 86(8):579–589. https://doi.org/10.1007/s00190-011-0537-0

Geng J, Wen Q, Zhang Q, Li G, Zhang K (2022) GNSS observable-specific phase biases for all-frequency PPP ambiguity resolution. J Geod. https://doi.org/10.1007/s00190-022-01602-3

Henkel P, Wen Z, Günther C (2010) Estimation of satellite and receiver biases on multiple Galileo frequencies with a Kalman filter. In: Proceedings of the 2010 International Technical Meeting of the Institute of Navigation, San Diego, pp 1067–1074

Heroux P, Kouba J (1995) GPS precise point positioning with a difference. In *Paper presented at Geomatics '95*, Ottawa

Hou P, Zhang B (2023) Decentralized GNSS PPP-RTK. J Geod. https://doi.org/10.1007/s00190-023-01761-x

Kalman RE (1960) A new approach to linear filtering and prediction problems. ASME J Basic Eng 82(1):35–45

Khodabandeh A (2021) Single-station PPP-RTK: correction latency and ambiguity resolution performance. J Geod. https://doi.org/10.1007/s00190-021-01490-z

Khodabandeh A, Teunissen PJG (2015) An analytical study of PPP-RTK corrections: precision, correlation and user-impact. J Geod 89(11):1109–1132. https://doi.org/10.1007/s00190-015-0838-9

Khodabandeh A, Teunissen PJG (2017) On the impact of GNSS ambiguity resolution: geometry, ionosphere, time and biases. J Geod. https://doi.org/10.1007/s00190-017-1084-0

Khodabandeh A, Teunissen PJG, Psychas D (2023) On the problem of double-filtering in PPP-RTK. Sensors 23(1):229. https://doi.org/10.3390/s23010229

Komjathy A, Sparks L, Wilson BD, Mannucci AJ (2005) Automated daily processing of more than 1000 ground-based GPS receivers for studying intense ionospheric storms. Radio Sci. https://doi.org/10.1029/2005RS003279

Laurichesse D, Mercier F, Berthias JP, Broca P, Cerri L (2009) Integer ambiguity resolution on undifferenced GPS phase measurements and its application to PPP and satellite precise orbit determination. J Inst Navig 56(2):135–149. https://doi.org/10.1002/j.2161-4296.2009.tb01750.x

Li X, Zhang X, Ge M (2011) Regional reference network augmented precise point positioning for instantaneous ambiguity resolution. J Geod 85(3):151–158. https://doi.org/10.1007/s00190-010-0424-0

Mervart L, Lukes Z, Rocken C, Iwabuchi T (2008) Precise point positioning with ambiguity resolution in real-time. In: Proceedings of the 21st International Technical Meeting of the Satellite Division of the Institute of Navigation, ION GNSS 2008, Savannah

Odijk D, Teunissen PJG (2008) ADOP in closed form for a hierarchy of multi-frequency single-baseline GNSS models. J Geod 82:473. https://doi.org/10.1007/s00190-007-0197-2

Odijk D, Teunissen PJG, Khodabandeh A (2014) Single-Frequency PPP-RTK: Theory and Experimental Results. In: Rizos C, Willis P (eds) Earth on the edge: science for a sustainable planet. International Association of Geodesy Symposia, Vol. 139, Springer, Berlin, 10.1007/978-3-642-37222-3_75

Odijk D, Zhang B, Khodabandeh A, Odolinski R, Teunissen PJG (2016) On the estimability of parameters in undifferenced, uncombined GNSS network and PPP-RTK user models by means of S-system theory. J Geod 90(1):15–44. https://doi.org/10.1007/s00190-015-0854-9

Psychas D, Verhagen S (2020) Real-time PPP-RTK performance analysis using ionospheric corrections from multi-scale network configurations. Sensors 20(11):3012. https://doi.org/10.3390/s20113012

Psychas D, Khodabandeh A, Teunissen PJG (2022) Impact and mitigation of neglecting PPP-RTK correctional uncertainty. GPS Solut 26:551. https://doi.org/10.1007/s10291-021-01214-y

Steigenberger P, Hugentobler U, Loyer S, Perosanz F, Prange L, Dach R, Uhlemann M, Gendt G, Montenbruck O (2015) Galileo orbit and clock quality of the IGS Multi-GNSS Experiment. Adv Space Res 55(1):269–281. https://doi.org/10.1016/j.asr.2014.06.030

Teunissen PJG (1997) A canonical theory for short GPS baselines. Part IV: precision versus reliability. J Geod 71:513–525. https://doi.org/10.1007/s001900050119

Teunissen PJG (2007) Dynamic data processing: recursive least-squares, 2nd edn. Delft University Press, Delft

Teunissen PJG, Khodabandeh A (2015) Review and principles of PPP-RTK methods. J Geod 89(3):217–240. https://doi.org/10.1007/s00190-014-0771-3

Teunissen PJG, Montenbruck O (eds) (2017) Springer Handbook of Global Navigation Satellite Systems, 1st edn. Springer Cham. https://doi.org/10.1007/978-3-319-42928-1

Teunissen PJG, Odijk D, Zhang B (2010) PPP-RTK: results of CORS network-based PPP with integer ambiguity resolution. J Aeronaut Astronaut Aviat 42(4):223–230

Teunissen PJG, Khodabandeh A, Psychas D (2021) A generalized Kalman filter with its precision in recursive form when the stochastic model is misspecified. J Geod. https://doi.org/10.1007/s00190-021-01562-0

Wang K, Khodabandeh A, Teunissen PJG (2017) A study on predicting network corrections in PPP-RTK processing. Adv Space Res 60(7):1463–1477. https://doi.org/10.1016/j.asr.2017.06.043

Wübbena G, Schmitz M, Bagge A (2005) PPP-RTK: precise point positioning using state-space representation in RTK networks. In: Proceedings of the 18th International Technical Meeting of the Satellite Division of the Institute of Navigation, ION GNSS 2005, Long Beach, pp 2584–2594

Zha J, Zhang B, Liu T, Hou P (2021) Ionosphere-weighted undifferenced and uncombined PPP-RTK: theoretical models and experimental results. GPS Solut. https://doi.org/10.1007/s10291-021-01169-0

Zhang B, Teunissen PJG, Odijk D (2011) A novel un-differenced PPP-RTK concept. J Navig 64(S1):S180–S191. https://doi.org/10.1017/S0373463311000361

Zhang B, Liu T, Yuan Y (2018) GPS receiver phase biases estimable in PPP-RTK networks: dynamic characterization and impact analysis. J Geod 92(6):659–674. https://doi.org/10.1007/s00190-017-1085-z

Zumberge JF, Heflin MB, Jefferson DC, Watkins MM, Webb FH (1997) Precise point positioning for the efficient and robust analysis of GPS data from large networks. J Geophys Res 102(3):5005–5017. https://doi.org/10.1029/96JB03860